V. Conclusions

The feasibility of applying the nonorthogonal FDTD algorithm to analyze nonrectangular via discontinuities was demonstrated, and the transient analysis of the equivalent circuit was analyzed with the help of window filters. To help eliminate the effects of the inaccurate higher frequency components in the time-domain waveforms, the Hanning window was employed with the result that more realistic time-domain waveform behavior was obtainable for qualitative analysis.

References

[1] S. Maeda, T. Kashiwa, and I. Fukai, "Full wave analysis of propagation characteristics of a through hole using the finite-difference time-domain method," *IEEE Trans. Microwave Theory Tech.*, vol. 39, pp. 2154–2159, Dec. 1991.

[2] K. S. Yee, "Numerical solution of initial boundary value problems involving Maxwell's equations in isotropic media," *IEEE Trans. Antennas Propagat.*, vol. AP-14, pp. 302–307, May 1966.

[3] P. H. Harms, J. F. Lee and R. Mittra, "A study of the nonorthogonal FDTD method vs. the conventional FDTD technique for computing resonant frequencies of cylindrical cavities," *IEEE Trans. Microwave Theory Tech.*, vol. 40, pp. 741–746, Apr. 1992.

[4] J. F. Lee and R. Mittra, "Finite difference time domain algorithm for nonorthogonal grids," Technical report, Electromagnetic Communication Lab., Department of Electrical and Computer Engineering, University of Illinois at Urbana-Champaign, 1991.

[5] J. F. Lee, R. Palandech and R. Mittra, "Modeling three-dimensional waveguide discontinuities using FDTD algorithm in curvilinear coordinate system," *IEEE Trans. Microwave Theory Tech.*, vol. 40, pp. 346–352, Feb. 1992.

[6] M. Fusco, "FDTD algorithm in curvilinear coordinates," *IEEE Trans. Antennas Propagat.*, vol. 38, pp. 76–89, Jan. 1990.

[7] M. A. Fusco, M. V. Smith, and L. W. Gordon, "A three-dimensional FDTD algorithm in curvilinear coordinates," *IEEE Trans. Antennas Propagat.*, vol. 39, pp. 1463–1471, Oct. 1991.

[8] R. Holland, "Finite-Difference solution of Maxwell's equations in generalized nonorthogonal coordinates," *IEEE Trans. Nucl. Sci.*, vol. NS-30, no. 6, pp. 4589–4591, Dec. 1983.

[9] W. D. Becker, P. Harms and R. Mittra, "Time domain electromagnetic analysis of interconnects in a multilayer computer chip package," accepted for publication in *IEEE Trans. Microwave Theory Tech.*, Special Issue.

[10] T. S. Blazeck and R. Mittra, "Transient analysis of lossy multiconductor transmission lines in nonlinear circuits," *IEEE Trans. Comp. Hybrids Manuf. Technol.*, vol. CHMT-14, no. 3, pp. 618–627, Sept. 1991.

[11] A. V. Oppenheim and R. W. Schafer, *Discrete-Time Signal Processing*. Englewood Cliffs, NJ: Prentice-Hall, 1989.

Slab Line Impedances Revisited

E. Costamagna, A. Fanni, and M. Usai

***Abstract*—Accurate solutions for impedances and charge distributions in slab lines and rectangularly shielded lines are obtained by numerical inversion of the Schwarz–Christoffel (SC) conformal transformation. Circular inner conductors are considered, putting to the test the relatively simple numerical methods we have utilized, and results are successfully compared to the best data available from the literature. The method, besides supplying accurate global parameters, such as capacitances and impedances, is also shown to provide good evaluations for local charge densities. Equipotential and field lines can be easily derived, and accurate calculation of local field maps is shown possible, even from approximate geometries, when boundary conditions are not completely known.**

I. Introduction

Powerful conformal mapping techniques by means of numerical inversion of the Schwarz Christoffel formula have already been described in [1] and [2], and successful applications to various structures of TEM transmission lines have been presented in [3]–[7]. In particular, relatively simple algorithms, as described in [2], have been shown suitable to cope with complex geometries, including curved conductor boundaries approximated by polygons with large number of sides. Moreover, accurate results have been derived in the application to domains with partially undefined boundaries, by imposing suitable magnetic walls where the flux line shape can be easily guessed.

The same algorithms give us the possibility of revisiting slab lines and rectangularly shielded lines with circular inner conductors, for which several results have been already provided both by exact solutions and approximate numerical calculations. In [8] and [9] a moments method with a point matching technique was employed to compute even- and odd-mode impedances and coupling coefficients for coupled slab lines; in [10] rectangularly shielded lines were analysed by a Carleman–Vekua method; in [11] a moment method combined with an image-mode Green's function was proposed, and the results include surface charge densities on the conductors of coupled slab lines. An extensive survey of available data for slab lines and related structures is supplied by Gunston [12, ch.4], and several TEM transmission lines with rectangular inner or outer conductors have already been analyzed by means of numerical conformal mapping in [6] and [7].

The various structures considered in this paper can be derived from the open sided, coupled slab line geometry in Fig. 1: two cylindrical rods are placed symmetrically between two parallel ground planes. Even- and odd-mode capacitances and impedances are computed by introducing electric or magnetic walls orthogonally to the ground planes midway between the rods, thus defining a through line geometry; unscreened and rectangular outer conductor slab lines are derived by considering a single rod and open or electric wall sides.

II. Single Line and Coupled Line Impedances

Single rod line impedances are considered first. A large amount of data are provided by Gunston: see [12, Table 4.1] for rectangular outer conductors and Table 4.3 for unscreened slab lines. Impedances

Manuscript received Dec. 30, 1991; revised May 7, 1992.

The authors are with the Istituto di Elettrotecnica, Universita di Cagliari, Piazza D'Armi, 09123 Cagliari, Italy.

IEEE Log Number 920413.

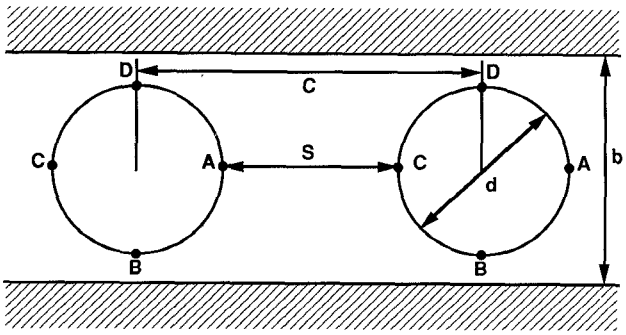

Fig. 1. Configuration of two-conductor slab-lines.

TABLE I
CAPACITANCES OF A SINGLE ROD BETWEEN PARALLEL PLANES (OPEN SIDES) AND CENTERED IN A RECTANGULAR OUTER CONDUCTOR (SHIELDED): d IS THE ROD DIAMETER, b IS THE DISTANCE BETWEEN TOP AND BOTTOM PLANES, c IS THE WIDTH OF THE RECTANGLE

		Present work Open sides	[11, Tab. I]	Present work Shielded	[10, Tab I]
d/b	c/b	C/2ε	C/2ε	C/2ε	C/2ε
0.8	2.3	7.432	7.378	7.462	
0 6	2 1	4.241	4.249	4.268	4.268
0.4	1 9	2.718	2 730	2 742	2.742
0.2	1.7	1.697	1.707	1.715	1 715
0.1	1.6	1.235	1.242	1.248	

computed following [2] have already been shown to be in very good agreement with Gunston's Table 4.1 and other data in [6, Tables 4, 5, 6], for various ratios of the outer conductor dimensions. For the open sided cases, good agreement has been found with all the data quoted by Gunston in Table 4.3 (from Wheeler, Knight, Frankel, Chisholm, Mahapatra and Lin and Chug), and differences do not exceed 0.03% compared to the "virtually exact" values quoted from Wheeler and Knight for d/b $\leq$ 0.9.

Some results are provided in [10, Table I] for shielded case and in [11, Table I] for the open sided case: again the agreement with our conformal mapping data is very good, as can be seen in Table I.

For coupled line structures, accurate self and coupling capacitance data have been available for some time in both numerical and graphical form, in particular in [13]. We limit our comparison to some numerical data.

In Table II even- and odd-mode geometrical capacitances are successfully compared with the values reported in [10, Table II], [11, Table II] and [14, Table I]. A broad range of d/b ratios is considered in [8, Tables I and II]: maximum differences between our even- and odd-mode impedance values and Stracca's *et al.* are limited to about 0.06% (which is the comparison accuracy achievable with the published four-figure data), except for two odd-mode cases, where differences were of about 0.1 and 0.2%.

Circular conductors have been approximated with polygons having number of sides ranging from 50 to 100; in the case of the comparison with [8], both 50 and 80 sides have been employed in the most critical cases and the results coincide with at least four figures. Their accuracy can be further checked by computing the coupling coefficients, involving small differences between even- and odd-mode impedances: the results appear in Fig. 2, and allow to successfully extend the range of curves, with respect to the range considered in [9], for at least three decades.

III. CHARGE DENSITIES AND FIELD MAPS

In the above calculations, the SC formula has been inverted to provide transformation from the analyzed geometry into the real axis of an intermediate complex plane, and then directly applied to provide

TABLE II
CAPACITANCES OF TWO-ROD CONFIGURATIONS

		Present work		Chisholm / McDermott [14, Tab. I]		Levy [14, Tab. I]		Fikioris & Tsalamengas [10, Tab. II]		Tai Lu & Olesen [11, Tab. II]	
		C/ε	C/ε	C/ε	C/ε	C/ε	C/ε	C/ε	C/ε	C/ε	C/ε
d/b	s/b	even	odd	even	odd	even	odd	even	odd	even	odd
0.354	0.176	3.9137	7.5506	3.9142	7.5347	3.9153	7 5528	3.9132	7 5494	3 912	7 543
0.400	0.226	4.5052	7.5397	4.5093	7.5347	4.5080	7.5401	4.5043	7 5888		
0.436	0.280	5.0344	7.5472	5.0281	7.5347	5 032	7.5501	5 0332	7 5468		
0.462	0.338	5.4731	7.5347	5.4731	7.5347	5.4718	7 5371	5 4718	7.5343		
0.482	0.398	5.8465	7.5366	5.8497	7.5347	5 8446	7 5339	5.8455	7 5339		
0.498	0.462	6.1728	7.5464	6.1648	7.5347	6.1721	7.5436	6 1721	7.5451		
0.510	0.528	6.4404	7.5525	6.4257	7.5347	6.4380	7.5514	6 4399	7 5508		
0.518	0.596	6.6427	7.5384	6.6404	7.5347	6 6424	7 5371	6.6421	7 5366		
0.534	0.806	7.0741	7.5369	7.0727	7.5347	7.0710	7.5359	7.0721	7 5361		
0.544	1.168	7.3833	7.5322	7.3855	7.5347	7.3806	7.5285	7.3819	7 5304	7.388	7 535
0 400	0.080	4.1657	11.2405	4.1646	11.0783	4.1553	11.2882	4.1651	11.2371	4 167	11.240
0.400	0.120	4.2641	9.5140	4.2631	9.4595	4 2626	9.5317	4.2634	9.5118	4.265	9.558
0.400	0.160	4.3587	8.5167	4.3578	8.4935	4.3516	8.5919	4.3579	8 5152		
0 400	0.200	4.4489	7.8594	4.4483	7.8478	4.4444	7.8652	4.4481	7.8584		
0.400	0.240	4.5346	7 3924	4.5340	7.3863	4.5358	7.3982	4.5337	7 3917		
0.400	0 400	4 8273	6 3905	4 8273	6.3903	4.8263	6.3914	4.8265	6 3903		
0 400	0 600	5 0821	5 8856	5 0826	5.8862	5.0819	5.8848	5.0818	5.8848		
0 400	0.760	5.2131	5.6947	5.2134	5.6949	5.2130	5 6946	5.2128	5 6940	5.217	5.700

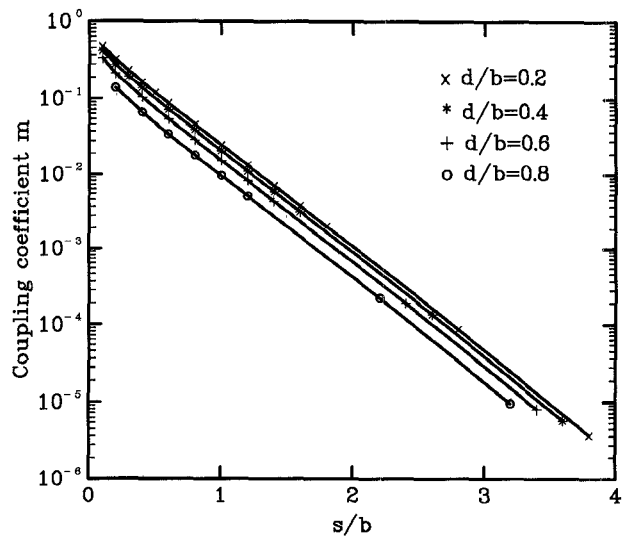

Fig. 2. Computed $(x, *, +, o)$ and linearly interpolated values for the coupling coefficient.

further transformation from this real axis into a rectangle, in which opposite sides are electric or magnetic walls and capacitances are readily evaluated.

The sides of the analyzed geometry which lie on electrodes are mapped into this rectangle with lengths which account for the side charges: in the limit, reducing side lengths, local charge densities can be accurately evaluated.

The number of sides used here to accurately describe the conductor boundaries lead to charge density evaluations which appear to be suitable for many practical purposes. As an example, consider the structure of Fig. 1. Side charges for the rod electrodes have been computed, representing the rods with 80-side regular polygons, and actual charge points have been plotted in Fig. 3 after suitable normalization. Comparison of these curves with Fig. 2 in [10] reveals negligible differences, at least at the draw level, except on the right side of Fig. 3(a). In this region, our curve 2 is higher than curve 3, instead of lower as in [11, Fig. 2(a)]. Note that, for curve 1, dimensions of s/b = 1 have been assumed, instead of s/b = 1.06, as reported in [11], probably due to a typing error.

When the parameters of the two SC formulas leading from the intermediate complex plane to the analyzed structure and to the final rectangle are known, it is very easy to map any defined pattern from one geometry to the other, and methods are described in [1] and [2].

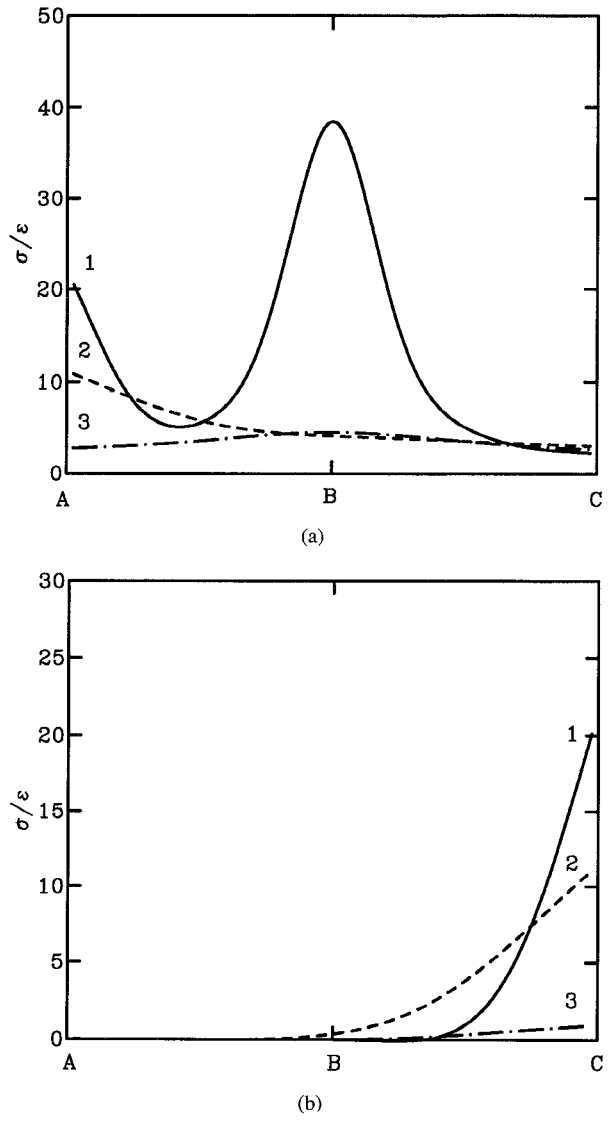

Fig. 3. Surface charge densities on the conductors of Fig. 1. The voltage on the first conductor is 1V; the second conductor and the two conducting planes are grounded. (a) First conductor; (b) second conductor. (1) d/b = 0.96, s/b 1.00; (2) d/b = 0.40, s/b = 0.48; (3) d/b = 0.544, s/b = 1.168.

Equipotential and flux lines can be determined in the rectangle by inspection, and it seems worth discussing application of the simple mapping predictor-corrector techniques of [2]. Consider for instance the structure shown in [10, Fig. 3], which is reported in Fig. 4. Rectilinear magnetic walls CD and EF have been imposed, normal to the outer and inner conductors in a region where flux line patterns can be easily divined, and an accurate map of the boundary ABCDEFGH has been obtained by mapping into infinity the side AH; twenty-four side poligons have been assumed to represent the inner conductor. The same equipotential and field lines considered in [10] have been derived and they are undistinguishable from that plotted in [10, Fig. 3] (see Fig. 4, continuous lines).

A predictor-corrector algorithm (from the rectangle to the intermediate complex plane) and the Heun algorithm (from the intermediate to the analysed geometry plane) have been applied as in [2] by segmenting patterns into 200, 500, and 1000 parts. Errors in the obtained maps, evaluated from the distance between the actual end point and its due position (when known) are of the order of 0.05% of the inner conductor diameter with 1000 segment patterns; they double

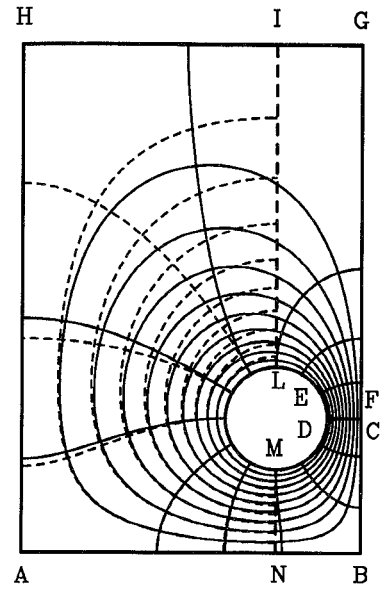

Fig. 4. Equipotential and flux lines of shielded single conductor line. Dashed lines are derived from arbitrarily imposed boundary magnetic walls.

or quadruple with 500 or only 200 segments. More significantly, it can be noted that equipotential and field lines start and end on the real axis of the intermediate plane: accuracy can be appreciated by noting that the end points of 1000 segment patterns are found in this plane at a distance from the real axis of the order of 1/10 of the length of their last segment.

Nevertheless, straightforward definition of the boundary to be mapped, as for the above CD and EF magnetic walls, is not always possible; sometimes, the actual structure cannot be accurately mapped using the simple methods in [2].

The first problem is not insurmountable in most practical cases: conformal mapping of approximate geometries have already been considered in [14], and methods to analyze structures by assuming approximate magnetic walls boundaries with some error evaluations have been presented in [3] and [5]. To show that useful results can be derived, at least for significant regions of actual structures, local errors have been stressed by imposing incongruous magnetic walls in Fig. 4 on the segments IL and MN, and the new HILMNA geometry has been analyzed.

As expected, in proximity of the imposed magnetic walls, equipotential and flux lines look very different from the previous exactly computed ones (see Fig. 4, dashed lines), but a large region can be recognized where fields are relatively unperturbed and correct pattern shapes are retained.

This suggests an approach to the second problem, i.e., to consider partial geometries, defined with some overlap near the fictitious boundaries, which are normally easily managed by the conformal mapping procedure.

IV. Conclusions

Slab line structures have been revisited, and results from various analysis methods have been compared with capacitance or impedance values derived from Schwarz–Christoffel conformal mapping, and very good agreement has been found.

In addition, surface charge densities evaluation and field map assessment via conformal mapping have been briefly discussed. Some topics related to partial mapping and to the defined geometries have also been dealt with.

REFERENCES

[1] L. N. Trefethen, "Numerical computation of the Schwarz–Christoffel transformation,"*SIAM J. Sci. Statist. Comput.*, vol. 1, no. 1, pp. 82–102, Mar. 1980.

[2] E. Costamagna, "On the numerical inversion of the Schwarz–Christoffel conformal transformation,"*IEEE Trans. Microwave Theory Tech.*, vol. MTT-35, pp. 35–40, Jan. 1987.

[3] —— "TEM parameters of angular offset strip lines," *Alta Frequenza*, vol. LVII, no. 5, pp. 193–201, May 1988.

[4] —— "Numerical conformal transformation of three magnetic wall structures," *IEEE Trans. Microwave Theory Tech.*, vol. 37, pp. 1263–1266, Aug. 1989.

[5] E. Costamagna, and A. Fanni, "Characteristic impedances of coaxial structures of various cross section by conformal mapping," *IEEE Trans. Microwave Theory Tech.*, vol. 39, pp. 1040–1043, June 1991.

[6] —— "Asymmetric TEM cell impedance calculation," *Proc. Inst Elec. Eng.*, vol. 137, pt. H, no. 5, pp. 318–320, Oct. 1990.

[7] —— "Analysis of rectangular coaxial structures by numerical inversion of the Schwarz–Christoffel transformation," *Proc. 8th COMPUMAG Conf.*, Sorrento, July 1991, pp. 573–576, *IEEE Trans Magn.*, vol. MAG-28, pp. 1454–1457, Mar. 1992.

[8] G. B. Stracca, G. Macchiarella, and M. Politi, "Numerical analysis of various configurations of slab lines." *IEEE Trans. Microwave Theory Tech.*, vol. MTT-34, pp. 359–363, Mar. 1986.

[9] —— G. Dolci, M. Politi, and G. Macchiarella, "Design formulas for coupled slab lines," *Alta Frequenza*, vol. LIV, no. 6, pp. 346–352, Dec. 1985.

[10] J. G. Fikioris and J. L. Tsalamengas, "Exact solutions for rectangularly shielded lines by the Carleman–Vekua method," *IEEE Trans. Microwave Theory Tech.*, vol. 36, pp. 659–675, Apr. 1988.

[11] I. Tai Lu and R. L. Olesen, "Analysis of transmission line structures using a new image-mode Green's function," *IEEE Trans. Microwave Theory Tech.*, vol. 38, pp. 782–785, June 1990.

[12] M. A. R. Gunston, *Microwave Transmission Line Impedance Data*. London: Van Nostrand Reinhold, 1972.

[13] E. G. Cristal, "Coupled circular cylindrical rods between parallel ground planes," *IEEE Trans. Microwave Theory Tech.*, vol. MTT-12, pp. 528–539, July 1964.

[14] R. Levy, "Conformal transformations combined with numerical techniques, with applications to coupled-bar problems," *IEEE Trans. Microwave Theory Tech.*, vol. MTT-28, pp. 369–375, Apr. 1980.

A Note on Experimental Determination of Small-Signal Equivalent Circuit of Millimeter-Wave FETs

A. Eskandarian and S. Weinreb

***Abstract*—New expressions for determination of the parasitic inductances L_g, L_d, and L_s in the small-signal equivalent circuit of high-frequency Field Effect Transistors (FET's) are derived, based on the "active/passive" (also known as "hot/cold") measurement technique developed in literature. These equations are required when the size of parasitic capacitances is such that their effect on the forward-biased gate measurement cannot be ignored, as has been the case with our millimeter-wave transistors. The method produces an equivalent circuit which has been used successfully for design of multi-stage amplifiers at 60 and 94 GHz.**

Manuscript received July 22, 1991; revised Apr. 23, 1992.

The authors are with Martin Marietta Laboratoriers/Gamma Monolithics (Partnership of Martin Marietta and Alpha Industries), Baltimore, MD 21227-3898.

IEEE Log Number 9204012.

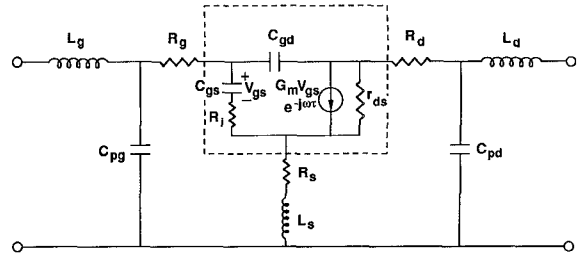

Fig. 1. The small-signal equivalent circuit of the FET's including the parasitic elements. The intrinsic FET model is shown in the dashed box.

I. INTRODUCTION

The most common method for determination of the equivalent circuit of a microwave Field Effect Transistor (FET) has been through minimization of the difference between measured and computed S-parameters versus frequency. However this procedure may not produce unique element values for the equivalent circuit and the dependence of element accuracy upon measurement accuracy is unclear. Dambrine *et al.* [1] and Berroth and Bosch [2], [3] recently presented methods that include S-parameters of the FET biased into a "passive" state, such as pinch-off or forward-biased gate, to provide additional data on the equivalent circuit. With this additional data it is possible to uniquely determine equivalent circuit values from measurements at a *single frequency*. Multiple-frequency measurements can then be utilized to test the accuracy of the data and the correct topology of the equivalent circuit as manifested by invariance of the element values with frequency.

The purpose of this letter is to make a necessary addition to the equations given in [1]–[2] and present experimental data showing invariance of equivalent circuit values from 1 to 18 GHz.

II. BACKGROUND

In "active/passive" measurement techniques, the equivalent circuit is conceptually divided into intrinsic and extrinsic parts. In a commonly used FET equivalent circuit shown in Fig. 1, the intrinsic part is shown in a dashed box. The extrinsic part includes the parasitic elements, i.e., the source, drain and gate resistances, and any additional inductances or capacitances which may exist due to the device layout, via holes, bonding pads, etc.

The parasitic elements are determined from the "passive" FET measurements, where the FET is biased similar to a diode, i.e., with zero voltage on the drain terminal. In this mode of operation the intrinsic part of the FET model in Fig. 1 should be replaced with an appropriate diode model that will depend on the bias voltage on the gate. Two types of gate biasing can be employed.

In the first type, a gate bias is chosen such that the channel under the gate is completely pinched off. This usually means a negative gate voltage. The drain and source terminals are at zero potential. The capacitive components of the equivalent circuit are dominant under this bias condition. The circuit diagram for this case is shown in Fig. 2, where it is assumed that the gate-source and gate-drain capacitances are equal to C_b (actually, depending on the lay-out structure of a FET, there is a small difference between these two capacitances). The measured S-parameters show capacitive behavior and are converted to Y-parameters. The value of C_b is determined from the imaginary part of Y_{12}. The values of C_{pd} and C_{pg} can then be determined from the imaginary parts of Y_{22} and Y_{11} simply by removing the contribution of C_b to these Y-parameters.